Numeric exploration of Non-trivial emergent phenomena in Quark-Gluon Plasma

Nia O'Callaghan[1] **and WA Horowitz**[1,2]

[1] Department of Physics, University of Cape Town, Rondebosch 7701, South Africa
[2] Department of Physics, New Mexico State University, Las Cruces, New Mexico, 88003, USA

E-mail: OCLJON001@myuct.ac.za

Abstract. We present here an analysis of probe quark behavior in a thermal Quark-Gluon Plasma via the AdS/CFT correspondence, modeling them as string endpoints with specific boundary conditions. We study both heavy (on-mass-shell) and light (off-mass-shell) quarks initially at rest, exploring analytic solutions where possible and using Wolfram's *Mathematica* for numerical solutions elsewhere. This enables comparison and verification. Due to difficulties in obtaining these numeric string solutions, we also examine numerical solutions for a point particle in the same spacetime geometries as a simpler test case. Although not all objectives were achieved, we present our findings, discuss limitations, and outline future research directions.

1 Introduction

The study of Quark-Gluon Plasma (QGP) advances our understanding of the quantum universe, especially the strong force and particle dynamics. Found in heavy ion collisions at RHIC and LHC, QGP is a complex, deconfined state of matter that challenges previous assumptions of a gas-like behavior, as evidenced by anisotropic momentum distribution (known as *elliptic flow*, [1, 2]). Both weak and strong coupling regimes are supported: perturbative QCD effectively predicts high transverse momentum observables [3] assuming weak coupling, while near-ideal hydrodynamics describes low transverse momentum observables [4, 5] assuming strong coupling.

Our investigation focuses on probe quarks interacting with QGP, modeled via AdS/CFT as strings in a String Theory. We aim to solve the string equations of motions allowing us to analyze the mean and RMS displacements of string endpoints, reflecting probe quark motion. Due to limited analytic solutions, we develop numerical solutions in Wolfram's *Mathematica*, validating with known cases. Additionally, we examine motion of point particles in the same spacetime geometries as a simplified approach to inform our methods and address challenges in the full string analysis.

2 The String Case

2.1 Theory

As established in Section 1 , we are ultimately interested in solving the equations of motion for a string in Anti-de Sitter or *AdS* spacetime for the purposes of connecting this motion to that of a probe quark via the AdS/CFT correspondence [6, 7]. More specifically, we want to solve the equations of motion arising from the Polyakov [8, 9, 10, 7] action,

$$S_P = -\frac{T}{2}\int_{\mathcal{M}} d^2\sigma\,\sqrt{-h}h^{ab}G_{\mu\nu}\partial_a X^\mu \partial_b X^\nu = -\frac{T}{2}\int_{\mathcal{M}} d^2\sigma\,\sqrt{-h}h^{ab}\gamma_{ab}\,, \tag{1}$$

where T is the string tension, $\mathcal{M}$ is the worldsheet of the string with coordinates $\sigma^a = (\tau, \sigma)^a$ and volume element $d^2\sigma = d\tau d\sigma$ (indexed with Latin indices to distinguish them from target spacetime objects, which are indexed with

Greek indices), $X^\mu = X^\mu(\tau, \sigma)$ are the coordinates of the string (to be understood as mapping functions from the string worldsheet to the target spacetime), $\gamma_{ab} = G_{\mu\nu}\partial_a X^\mu \partial_b X^\nu$ is the metric induced on the worldsheet by the pullback of the target spacetime metric $G_{\mu\nu}$ along the mapping functions X^μ, h_{ab} is the metric on the worldsheet itself (with inverse h^{ab} and determinant h), and natural units are used unless otherwise stated. The equations of motion resulting from the extremization of (1) are

$$\nabla_a \Pi^a_\mu - \Gamma^\alpha_{\mu\nu}\Pi^a_\alpha \partial_a X^\nu = 0 \tag{2}$$

where $\Pi^a_\mu = -Th^{ab}G_{\mu\nu}\partial_b X^\nu$ are the canonical momentum densities obtained from the action (1) via the usual procedure, $\Gamma^\alpha_{\mu\nu}$ are the usual Christoffel symbols of the target spacetime metric $G_{\mu\nu}$, and ∇_a is the covariant derivative on the string worldsheet from the Levi-Civita connection associated with the worldsheet metric h_{ab}.

Our goal is to solve these equations of motion for two cases of open strings, the first with both endpoints fixed (corresponding to a heavy, on-mass-shell probe quark) and the second with one endpoint fixed and the other free (corresponding to a light, off-mass-shell probe quark), and we will refer to these two cases as the "heavy" and "light" cases respectively [7, 11]. Ultimately we want to consider the $AdS_5 \times S^5$ spacetime geometry as this is dual to $\mathcal{N} = 4$ Super Yang-Mills CFT[1], however no analytic solutions exist in this case. We will therefore consider the simpler spacetime geometry of AdS_3-Schwarzschild, where analytic solutions to equation (2) are present[2]. This will allow us to compare the obtained numeric solutions to these analytic solutions in order to establish the validity of our numeric solutions before proceeding to the more complex spacetime geometry.

2.2 Numeric Results

Making use of the *NDSolve* function build into Wolfram's *Mathematica* to numerically solve equation (2) in the above established spacetime geometry, we are able to obtain numeric solutions in both the heavy and light cases. Figure 1 shows parametric plots of the radial component $X^1(\tau, \sigma) = r(t, \sigma)$ of these solutions in the static gauge, along with plots of the corresponding analytic solutions.

The plots in Figure 1 show good agreement for the heavy case but significant deviation for the light case. Notably, the light case exhibits non-physical behavior: the shaded region in plot 1d indicates the string endpoint folding over itself, leading to that endpoint falling inwards faster than the analytic solution's inward fall at the local speed of light. This implies the numeric endpoint exceeds the local speed of light. The deviations are around one-tenth of the string length — much larger than numerical error alone could account for.

Due to these issues with obtaining a numeric solution for the string that agrees with the analytic solution, and being unable to remedy this issue via the usual approaches[3], we will instead consider the simpler problem of numerically solving for the motion of a point particle in the same spacetime geometry.

3 The Point Particle Case

3.1 Theory

The trajectory of a point particle is known as a geodesic of the spacetime it exists within. These geodesics can be understood as generalisations of the notation of a straight line[13, 14]; they are the paths that extremize the invariant spacetime interval between two events, analogous to how straight lines extremize the Euclidean distance between two points. Following this logic, we extremize the length functional

$$I = \int d\lambda \sqrt{-G_{\mu\nu}\frac{dx^\mu}{d\lambda}\frac{dx^\nu}{d\lambda}} = \int d\lambda \sqrt{-\dot{x}^2}, \tag{3}$$

where $\dot{x}^\mu = \frac{dx^\mu}{d\lambda}$, and the square of a vector is shorthand for the contraction of the vector with itself by the metric. From the functional (3) we derive the geodesic equation [13]

$$\frac{d^2x^\mu}{d\lambda^2} + \Gamma^\mu_{\nu\rho}\frac{dx^\nu}{d\lambda}\frac{dx^\rho}{d\lambda} = 0, \tag{4}$$

for a trajectory $x^\mu(\lambda)$ parameterised by an arbitrary (affine) parameter λ. In deriving equation (4), we have considered the parameterised path $x^\mu(\lambda)$ as an object in its own right, rather than as the physical trajectory of a particle,

[1] In the appropriate limiting cases, this field theory provides a good approximation for QCD [6, 12]

[2] Though these analytic solutions are derived by making use of the static ($X^0(\tau, \sigma) = \tau$) and conformal ($h_{ab} = \eta_{ab} = \mathrm{diag}(-1, 1)$) gauges.

[3] Specifically, neither re-forming the equations of motion nor adjusting the Working Precision, Accuracy Goal, Precision Goal, and/or Grid Spacing options supplied to *NDSolve* are able to resolve the numeric problems.

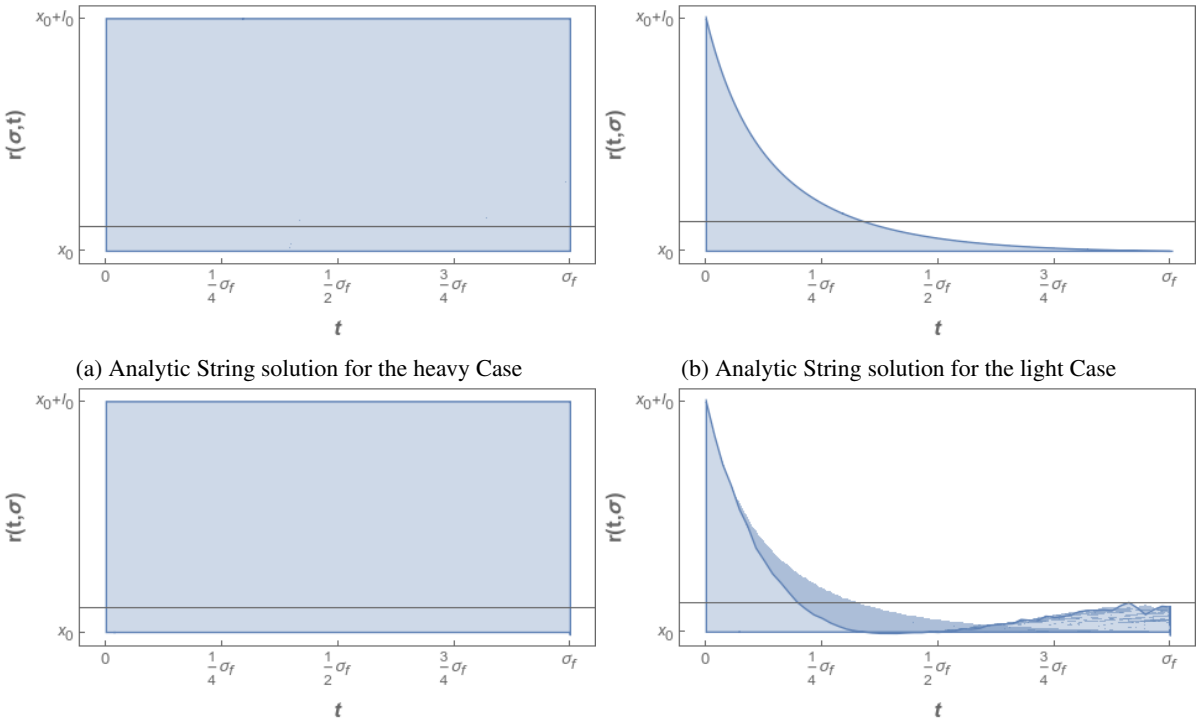

(a) Analytic String solution for the heavy Case

(b) Analytic String solution for the light Case

(c) Numeric String solution for the heavy Case

(d) Numeric String solution for the light Case

Figure 1: Parametric plots of the analytic (*top*) and numeric (*bottom*) string solutions in both the heavy (*left*) and light (*right*) cases. These plots show the full spacial extent of the string on the vertical axis, plotted over time on the horizontal.

but the switch to the latter is simple enough: We can take the action for a massive, relativistic point particle as simply being proportional[4] to the length of its worldline [13, 14, 10],

$$S_m = -m \int ds = -m \int d\lambda \sqrt{-G_{\mu\nu} \frac{dx^\mu}{d\lambda} \frac{dx^\nu}{d\lambda}}. \tag{5}$$

This action (5) is the point particle analogue to the Nambu-Goto action[5] for the string.

We can additionally consider the einbein action [8],

$$S_e = \frac{1}{2} \int d\lambda \left(\frac{\dot{x}^2}{e} - em^2 \right), \tag{6}$$

where $e = e(\lambda)$ is this new einbein object, an additional degree of freedom introduced in analogy to the intrinsic worldsheet metric[6] introduced in equation (1). This action (6) maintains reparameterisation invariance without the square root of equation (5) and applies to both massive and massless particles, unlike the S_m action which only works for massive particles. Additionally, a third point particle action can be derived by simplifying the length functional (3): by taking advantage of the monotonicity of the square root function we can, by "squaring" the functional I, obtain a new length functional I_2 and an associated action S_2 [13],

$$I_2 = \int d\lambda \, G_{\mu\nu} \frac{dx^\mu}{d\lambda} \frac{dx^\nu}{d\lambda} = \int d\lambda \, \dot{x}^2 \implies S_2 = m^2 \int d\lambda \, G_{\mu\nu} \frac{dx^\mu}{d\lambda} \frac{dx^\nu}{d\lambda} = m^2 \int d\lambda \, \dot{x}^2, \tag{7}$$

[4]The proportionality constant must clearly have dimensions of energy to ensure that this new functional (5) does actually have the dimensions of action, and what better to use than the mass of the particle being a constant property of it. The negative sign is then needed to ensure we recover the correct non-relativistic limit to the action.

[5]$S_{NG} = -T \int d^2\sigma \sqrt{-\det(\gamma_{ab})}$, where γ_{ab} is the induced metric on the string worldsheet, as in equation (1). This action is proportional to the area traced out by the string worldsheet.

[6]This analogy runs deeper than it at first appears, as equation (6) can be recast to show that the e acts as a one-dimensional metric on the worldline of the particle [8].

completely analogously to how the action S_m was obtained from the functional I. This action (7) is mathematically simpler, but this simplicity comes at the cost of reparameterisation invariance; we have effectively fixed the proper time parameterisation for our worldline in using the S_2 action [13]. Additionally, this action is also only valid for massive particles, much like the S_m action. For the massless case, we do have one additional method to solve for the trajectory of the particle aside from the extremization of equation (6) or the direct use of the geodesic equation (4), and this is to make use of the fact that massless particles must travel on lightlike or null trajectories. These trajectories satisfy $\dot{x}^2 = 0$ which, by making use of the static gauge $x^0(\lambda) = t(\lambda) = \lambda$, gives us a first order differential equation that can be solved to find $x^1(\lambda) = r(\lambda)$.

The equations of motion arising from all three actions[7] can be written as

$$\frac{D}{d\lambda}\pi_\mu^{(i)} = \dot{x}^\nu \nabla_\nu \pi_\mu^{(i)} = 0, \tag{8}$$

where $i \in \{m, e, 2\}$ is the same label as the subscript on the associated action, $\frac{D}{d\lambda} = \dot{x}^\nu \nabla_\nu$ is the parallel transport operator [13], and $\pi_\mu^{(i)}$ is the canonical momentum obtained from the corresponding action via the usual procedure. All the difference arising from the specifics of the different actions are contained within the different canonical momenta. In the case of the einbein action, we additionally need to consider the equations of motion for the einbein itself, which come out to be a constraint equation. These canonical momenta and this constraint equation are given in equations (9) and (10) respectively.

$$\pi_\mu^{(m)} = \frac{m\dot{x}_\mu}{\sqrt{-\dot{x}^2}}; \;\; \pi_\mu^{(2)} = 2m^2\dot{x}_\mu; \;\; \pi_\mu^{(e)} = e^{-1}\dot{x}_\mu; \tag{9}$$

$$0 = \frac{\dot{x}^2}{e^2} + m^2. \tag{10}$$

In all cases, we will use the initial conditions $x^\mu(0) = (t(0), r(0))^\mu = (0, 1)^\mu$ and $\dot{t}(0) = 1$. In the massive case, we will then use $\dot{r}(0) = 0$ and solve equation (10) to obtain possible values for $e(0)$, while for the massless case we will obtain $\dot{r}(0)$ from the other initial conditions to place the particle on a null trajectory at $\lambda = 0$. We will then attempt to numerically solve all versions of equation (8) from the different actions, variations on reforming these equation, variations on the form of equation (10) in the einbein case as well as its derivative, and with the options of $-1, 0,$ or 1 for $\dot{e}(0)$ in either case and $e(0)$ in the massless case. This leads to a huge number of different potential configurations for the numeric solutions which will be run via *NDSolve* and, once non-physical solutions have been ruled out[8], these solutions will be compared. Table (1) shows the final counts of the number of solution configurations, the number of non-physical solutions, the number of solutions that were not able to be solved, and the final count of remaining numeric solutions both in Minkowski spacetime and in two coordinate systems[9] for AdS_3-Schwarzschild spacetime [7, 11]. In all cases, we will take the metric to have the form $ds^2 = -f(r)dt^2 + g(r)dr^2$, which allows us to recover all three cases by the forms of $f(r), g(r)$[10].

3.2 Numeric Results

Due to the large number of variations on the solutions, it is not possible to generate a meaningful plot showing all the solutions and how they compare with each other. We have therefore instead opted to consider comparisons of individual solutions against one particular selected solution. Figure 2 shows this comparison between the solution obtained from the geodesic equation[11] and a sample solution[12] generated using the equations of motion arising from the einbein action (6), in the form of a ratio[13] between the two solutions.

---

[7] That is, from S_m in equation (5), from S_e in equation (6), and from S_2 in equation (7).

[8] Solutions are deemed non-physical and ruled out if they either do not satisfy at least one of the initial conditions laid out above, or else if the solution for the time coordinate has $\dot{t}(\lambda) < 0$, as time must be an increasing function.

[9] Those being the usual (t, r) radial coordinate system, which we will refer to as "AdS" coordinates, and the tortoise coordinates (t, r_*) which transform the radial direction to put the metric into a conformally flat form where it is proportional to the Minkowski metric, and which we will refer to as such.

[10] Minkowski spacetime corresponds to $f(r) = g(r) = 1$, AdS_3-Schwarzschild spacetime in AdS coordinates by $f(r) = \frac{1}{g(r)} = f_{\text{AdS}}(r)$ and in tortoise coordinates with $f(r) = g(r) = f_{\text{Tort}}(r)$; where $f_{\text{AdS}}(r)$ and $f_{\text{Tort}}(r)$ are the usual AdS_3-Schwarzschild blackening factor in AdS and tortoise coordinates respectively

[11] For numeric reasons, the geodesic equation with lower μ index is preferred

[12] In both cases, the derivative of the einbein constraint equation (10) has been used rather than the constraint equation itself, and the same form of this equation is used in both cases. No initial conditions for $\dot{e}$ were given, and the initial condition $e(0) = \frac{\sqrt{f(r(0))}}{m}$ was used in the massive case, while the initial condition $e(0) = 0$ was used in the massless case.

[13] As shown in the axes labels of figure 2, it is not just the ratio of the two solutions that are plotted but the difference between this ratio and one, so that perfect agreement is given by zero.

	Minkowski		AdS		Tortoise		Final Count		
	M	Ml	M	Ml	M	Ml	M	Ml	Total
Initially	12	18	180	244	180	244	372	506	878
Failed to run	0	2	128	125	115	238	243	365	608
Non-physical	0	0	34	39	40	3	74	42	116
Finally	12	16	18	80	25	3	55	99	154

Table 1: Counts of the number of solutions available, computed, and ruled out, in Minkowski spacetime and in AdS and tortoise coordinates for AdS_3-Schwarzschild spacetime. The column labels "M" and "Ml" refer to the massive and massless particle cases respectively.

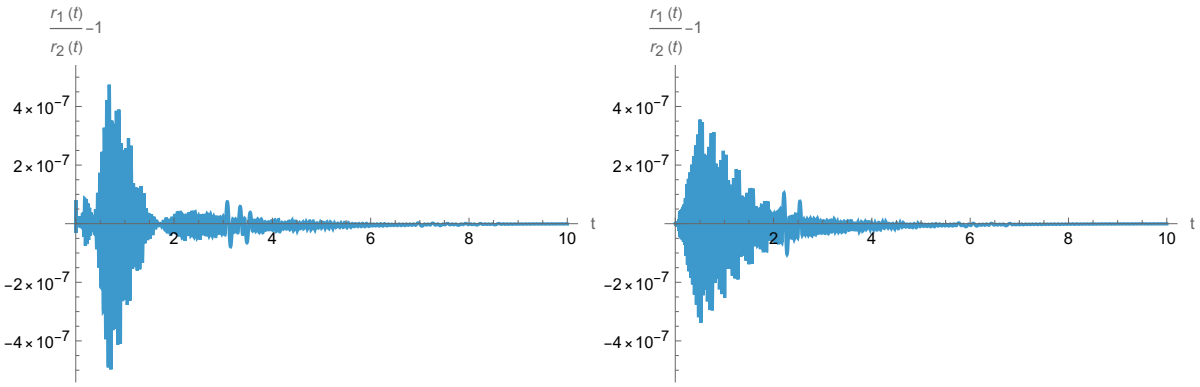

Figure 2: Ratio plots showing the comparison between the geodesic equation and a specific solution of the einbein equation of motion in AdS coordinates, which we will take as a representative example of the comparisons between solutions.

From the plots shown in figure 2, we see good agreement between the solutions in both cases — the plots have the same scale on the vertical which is of the order $\sim 10^{-7}$, much smaller than any length scale present in the problem (given by $r_H = 0.3$ and $r(0) = 1$).

Figure 2 compares a small subset of solutions; while most align on similar scales, some pairs show large discrepancies, indicating at least one solution is incorrect. By scoring each solution, we identify patterns and conditions under which solutions perform best; taken here to mean those that agree[14] with the most others. In the massive case, einbein equations of motion (using the derivative of the constraint and initial conditions for e) perform best, with some variations in the exact form of the equations and initial conditions across coordinate systems. Notably, solutions from the massive actions (S_m and S_2) all fail or are physically invalid, suggesting the solver struggles with these equations or that they contain subtle issues. In the massless case, null methods excel, followed by direct use of the geodesic equation. In tortoise coordinates, einbein solutions fail or are invalid, but in AdS coordinates, they yield physically meaningful results—particularly when configurations mirror those successful in the massive case—highlighting the potential significance of this specific configuration choice.

4 Conclusions and Outlook

From the analyses presented in Section 3.2, we can see that there is no choice of action for which the resulting equations of motion numerically perform best in all cases. Instead, the closest we have is that the geodesic equation (4) arising from the extremization of the length functional (7) seems to show good results in all cases, although it is not best performing in any of them. We also see that the usual massive point particle actions (5) and (7) do not result in equations that are numerically solvable; and while the einbein action (6) results in equations that are numerically solvable in *most* cases, they are not in all cases and even in the cases where they are, the solutions can be incredibly sensitive to the exact form of the constraint equation (or its derivative) and the choice of initial conditions for e and/or $\dot{e}$ used. Potential directions to pursue in the future include a more detailed examination of the reasons for why certain actions do not result in numerically solvable equations of motion, and why this sometimes

[14]Where we are taking agreement to mean no deviations larger than the arbitrarily chosen cutoff value of 10^{-5}

depends on the coordinate system used. Additionally, there is also the question of why the einbein solutions are so sensitive to initial conditions of the non-physical degree of freedom and the form of the constraint equation used for this degree of freedom, as well as if this sensitivity or the issues in obtaining numeric solutions are resolved by changing the precision or accuracy parameters of *NDSolve*. Finally then, since the geodesic equation shows good numerical solutions in all cases, it is potentially worth exploring a new comparison methodology of comparing all solutions to the geodesic equation rather than to all others, and if it is possible to obtain an analytic solution to this geodesic equation to obtain more detailed comparisons.

Returning to the string case, we can also use the insights obtained above in the point particle case to illuminate potential directions to proceed here. All string solutions presented here were obtained in the conformal gauge, but in the particle case we observe that the equations including an additional degree of freedom (there in the form of the einbein) generally performed better — by analogy, perhaps including additional non-physical degrees of freedom to be solved for in the string case will lead to better and more stable solutions. There is also the option of exploring the equations of motion obtained from the Nambu-Goto action, although this action is analogous to the massive action S_m in the particle case, indicating that we are unlikely to obtain useful solutions from this action unless we can determine the reason that the S_m and S_2 actions fail in the particle case and show those do not apply here. Finally then, we also have the option of using the obtained geodesic solutions from the point particle as seeds for the string solutions.

Acknowledgements
NO and WAH thank the National Research Foundation (NRF), the National Institute for Theoretical and Computational Physics (NITheCS), and the SA-CERN collaboration for their generous financial support during the course of this work.

References

[1] M. Gyulassy, "The qgp discovered at rhic," 2004.

[2] U. Heinz and P. Kolb, "Early thermalization at RHIC," *Nuclear Physics A*, vol. 702, no. 1-4, pp. 269–280, 5 2002. [Online]. Available: https://doi.org/10.1016\%2Fs0375-9474\%2802\%2900714-5

[3] A. Majumder and M. van Leeuwen, "The theory and phenomenology of perturbative QCD based jet quenching," *Progress in Particle and Nuclear Physics*, vol. 66, no. 1, pp. 41–92, 1 2011. [Online]. Available: https://doi.org/10.1016\%2Fj.ppnp.2010.09.001

[4] U. Heinz and R. Snellings, "Collective flow and viscosity in relativistic heavy-ion collisions," *Annual Review of Nuclear and Particle Science*, vol. 63, no. 1, pp. 123–151, 10 2013. [Online]. Available: https://doi.org/10.1146\%2Fannurev-nucl-102212-170540

[5] C. GALE, S. JEON, and B. SCHENKE, "HYDRODYNAMIC MODELING OF HEAVY-ION COLLISIONS," *International Journal of Modern Physics A*, vol. 28, no. 11, p. 1340011, 4 2013. [Online]. Available: https://doi.org/10.1142\%2Fs0217751x13400113

[6] J. Maldacena, "The large-n limit of superconformal field theories and supergravity," Apr 1999. [Online]. Available: https://link.springer.com/article/10.1023/A:1026654312961

[7] A. K. Mes, "Understanding heavy and light quark brownian motion from ads/cft," Master's thesis, University of Cape Town, 2020.

[8] D. Tong, "String theory," 2009. [Online]. Available: http://www.damtp.cam.ac.uk/user/tong/string.html

[9] A. M. Polyakov, "Quantum Geometry of Bosonic Strings," *Phys. Lett. B*, vol. 103, pp. 207–210, 1981.

[10] B. Zwieback, *A First course in String Theory*, 2nd ed. Cambridge University Press, 2009.

[11] R. W. Moerman and W. A. Horowitz, "A semi-classical recipe for wobbly limp noodles in partonic soup," 2016.

[12] G. Hooft, "A planar diagram theory for strong interactions," *Nuclear Physics B*, vol. 72, no. 3, pp. 461–473, 1974. [Online]. Available: https://www.sciencedirect.com/science/article/pii/0550321374901540

[13] S. M. Carroll, *Spacetime and Geometry: An Introduction to General Relativity*, hardcover ed. Cambridge University Press, 9 2019.

[14] D. Tong, "General relativity," 2019. [Online]. Available: https://www.damtp.cam.ac.uk/user/tong/gr.html